MICRO HYDRO POWER STATION WITH HYDRODYNAMIC ROTOR

PhD, assoc. prof. V. Bostan
Universitatea Tehnică a Moldovei

INTRODUCTION

The research of the systems for conversion of renewable sources of energy (RSE) and their elaboration is of great importance for Republic of Moldova being in complete agreement with European Union policies and commitments of the Republic of Moldova toward the increase of the RSE quote in the energy production up to 20% in 2020. Systems for conversion of the kinetic energy of the free water flow into electric or mechanical energy are using turbines in the absence of dams, thus eliminating the negative environmental impacts such as noise pollution, excessive sedimentation, low water quality, effects on aquatic fauna. The kinetic energy of free water flow is a recommended energy source available continuously and it can be efficiently harnessed by floatable micro-hydro power stations in order to meet the energy needs of consumers, particularly in remote rural areas. As working elements in such small-scale hydro-electric power stations are used Garman type rotors with oblique axis blades, Darrieus rotors, multi-blade rotors, Gorlov type turbines. The anchored power stations require a foundation to which the working elements, multiplicator and electric generator placed on a resistance frame are anchored. In contrast with anchored power stations, the floating micro-hydro power stations can be placed in the areas with higher flow rate and at further distances from the river banks. Moreover, they can be grouped and positioned appropriately to form a hydro power farm in order to convert more efficiently the flowing river kinetic energy. Nowadays, various types of floating micro-hydro power stations are being used with either horizontal or vertical axis.

Based on carried out research [1], there is proposed a constructive concept of two flow turbines with 3 and 5 blades with NACA hydrodynamic profile. These turbines have been used to design and manufacture four configurations of floatable micro hydro power stations for the conversion of river kinetic energy [2].

In order to increase the conversion efficiency it is necessary to optimize the hydrodynamic profile of the blades taking into account the turbine dimensions, angle of attack and exploitation conditions. Since conversion efficiency highly depends on the hydrodynamic profile of the blades, it is important to minimize the deformations of the blades due to hydrostatic pressure and applied forces. Therefore, it is important to design and analyze a resistance structure for the blades that will preserve the prescribed design shape parameters, along both the blade length and height.

2. TURBINE WITH HYDRODYNAMIC BLADES

Hydrodynamic rotor consists of main shaft 2 (fig.1), horizontal rods 1 and blades 4 with NACA 0016 hydrodynamic profile assembled in semi shaft 3 with the possibility to rotate around them. Under the action of hydrodynamic forces, the blades 4 rotate with angular velocity ω depending

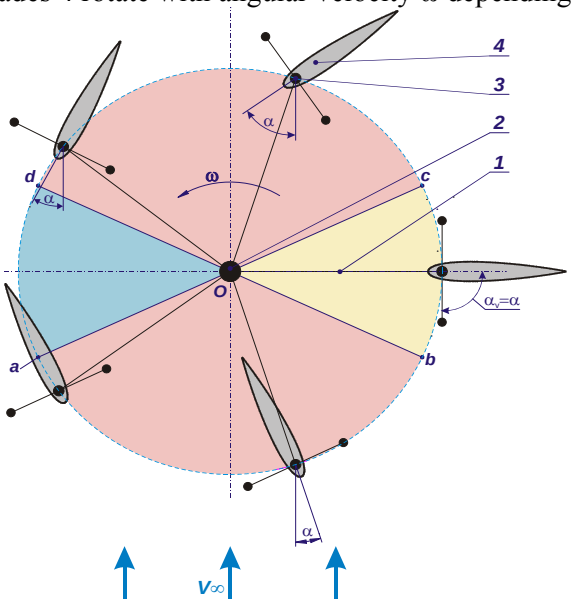

Figure 1. Conceptual scheme of vertical axis turbine with hydrodynamic blades.

on the water flow velocity $\vec{V}_\infty$, blades angle of attack α and rotor diameter D (diameter of location of blade semi shaft axes).

To identify the character of influence of hydrodynamic effects on a blade with NACA symmetric profile in its rotational motion around

centre *O*, four specific areas of blade-fluid interaction are defined: upstream area *Oab*, downstream area *Ocd*, transition from upstream to downstream area *Obc* and transition from downstream to upstream area *Oda*.

Maximum efficiency of flow kinetic energy conversion into useful mechanical energy can be realized if a blade with hydrodynamic profile contributes to the development of a total torque T_Σ under the action of hydrodynamic force during one complete rotation. To achieve this condition it is necessary that blades 3 be oriented under an optimum (from the point of view of conversion efficiency) angle of attack α with respect to the flow direction for each area crossed by every blade during its complete rotation.

3. DETERMINATION OF HYDRODYNAMIC COEFFICIENTS

Consider a blade with symmetric hydrodynamic profile placed in a water stream with uniform velocity $\vec{V}_\infty$ (fig. 2). In the fixing point O' of the symmetrical blade with rod OO' two coordinate systems are considered: $O'xy$ system with axis $O'y$ oriented in the direction of the velocity vector $\vec{V}_\infty$ and $O'x'y'$ system with axis $O'y'$ oriented along the rod OO'. Points A and B correspond to the trailing and the leading edges, respectively. The angle of attack α is the angle between the profile's chord AB and the direction of the velocity vector $\vec{V}_\infty$, and the positioning angle φ is the angle formed by the velocity vector direction and OO'.

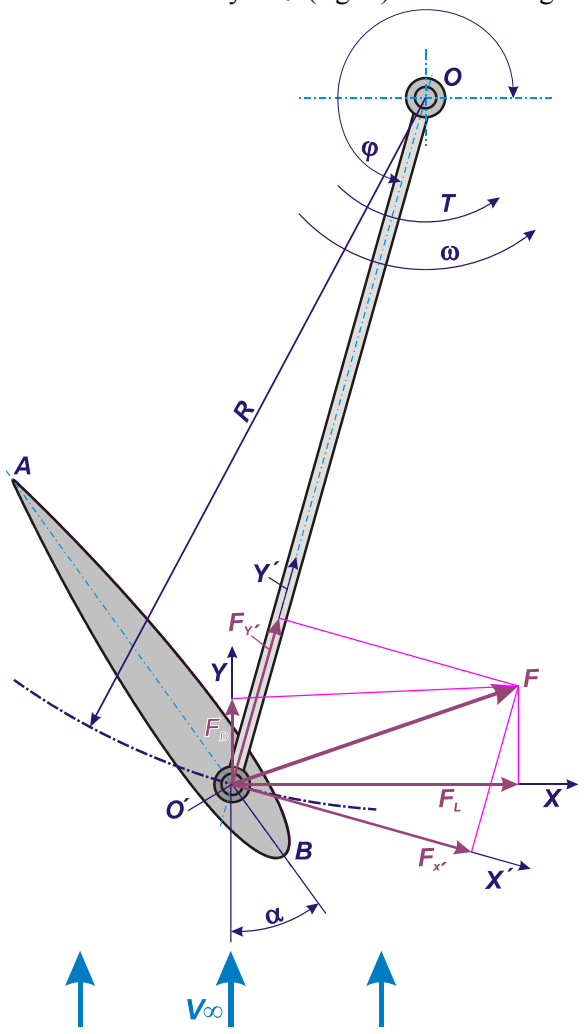

Figure 2. Hydrodynamic profile blade

The hydrodynamic force $\vec{F}$ has its lift and drag components in directions O'x and O'y, respectively, given by:

$$F_L = \frac{1}{2} C_L \rho V_\infty^2 S_p, \quad F_D = \frac{1}{2} C_D \rho V_\infty^2 S_p, \qquad (1)$$

where ρ is the fluid density, V_∞ is the flow velocity, $Sp=cH$ (c is the length of chord AB, and H is the blade height) represents the lateral surface area of the blade, and C_L and C_D are dimensionless lift and drag hydrodynamic coefficients. The hydrodynamic coefficients C_L and C_D are functions of the angle of attack α, Reynolds number Re and hydrodynamic shape of the blade. The symmetric shape of the hydrodynamic profile is chosen from the library of NACA 4 digits aerodynamic profiles and the profile chord length is considered unitary.

The components of hydrodynamic force in coordinate system $O'x'y'$ are:

$$\begin{aligned} F_{x'} &= -F_L \sin\varphi + F_D \cos\varphi, \\ F_{y'} &= F_L \cos\varphi + F_D \sin\varphi. \end{aligned} \qquad (2)$$

The torque developed by blade i at the rotor shaft O is

$$T_i = F_{x'} \cdot |OO'|, \qquad (3)$$

and the total torque developed by all blades is

$$T_\Sigma = \sum_{i=1}^{N_b} T_i, \qquad (4)$$

where N_b is the number of rotor blades.

In order to compute the lift hydrodynamic coefficient a panel method is being used. Thus, the fluid is considered incompressible and inviscid, and its flow plane and potential [3, 4]. The flow potential Φ in point $P'(x,y)$ is obtained by superposition of a uniform velocity flow, a distribution of sources with strength $q(s)$ and a distribution of vortexes with strength $\gamma(s)$ on profile C:

$$\Phi(P') = V_\infty x\cos\alpha + V_\infty y\sin\alpha + \oint_C \frac{q(s)}{2\pi}\ln(r)ds - \oint_C \frac{\gamma(s)}{2\pi}\theta ds, \quad (5)$$

where s denotes the arc length measured along profile C, and (r,θ) are the polar coordinates of P' relative to the point on C corresponding to arc length s.

The computation of the flow potential Φ uses a collocation method in which profile C is discretized with N boundary elements E_j with endpoints P_j and P_{j+1}. It is assumed that the vortex strength $\gamma(s)$ is constant, and the source strength $q(s)$ is piecewise constant on each boundary element E_j with value q_j, $j=1,\ldots,N$. Breaking the integrals in (5) along each element gives:

$$\Phi = V_\infty x\cos\alpha + V_\infty y\sin\alpha + \sum_{j=1}^{N}\int_{E_j}\left(\frac{q_j}{2\pi}\ln(r) - \frac{\gamma}{2\pi}\theta\right)ds, \quad (6)$$

where unknowns γ and q_j are determined from imposing boundary and Kutta conditions on collocation points $M_j\left(\bar{x}_j,\bar{y}_j\right)$ chosen to be the midpoints of E_j. Let u_j and v_j be velocity components in M_j. Boundary and Kutta conditions are:

$$\begin{aligned} &-u_j\sin\theta_j + v_j\cos\theta_j = 0,\ \mathrm{j}=1,\ldots,N \\ &u_1\cos\theta_1 + v_1\sin\theta_1 = -u_N\cos\theta_N + v_N\sin\theta_N, \end{aligned} \quad (7)$$

where θ_j denotes the angle formed by element E_j and x-axis. The velocity components in point M_i are determined by the contributions of velocities induced by sources and vortexes on each boundary element E_j:

$$\begin{aligned} u_i &= V_\infty\cos\alpha + \sum_{j=1}^{N}u_{ij}^{s}q_j + \sum_{j=1}^{N}u_{ij}^{v}\gamma, \\ v_i &= V_\infty\sin\alpha + \sum_{j=1}^{N}v_{ij}^{s}q_j + \sum_{j=1}^{N}v_{ij}^{v}\gamma, \end{aligned} \quad (8)$$

where $u_{ij}^{s}, v_{ij}^{s}, u_{ij}^{v}, v_{ij}^{v}$ are the influence coefficients.

Let β_{ij}, $i\neq j$, be the angle between P_jM_i and M_iP_{j+1}, and set $\beta_{ii}=\pi$. Let $r_{ij} = \left|M_iP_j\right|$ and define $D_{ij} = r_{i,j+1}/r_{ij}$. Boundary and Kutta conditions (7) together with equations (8) lead to a linear system with unknowns γ and q_j:

$$\left[A_{ij}\right]_{i,j=1}^{N+1}\begin{bmatrix} q_1 \\ q_2 \\ \vdots \\ q_N \\ \gamma \end{bmatrix} = \begin{bmatrix} b_1 \\ b_2 \\ \vdots \\ b_N \\ b_{N+1} \end{bmatrix} \quad (9)$$

with coefficients A_{ij} and b_i given by formulas with $i,j=1,\ldots,N$:

$$\begin{aligned} A_{ij} &= \frac{1}{2\pi}\left(\sin\Delta_{ij}\ln D_{ij} + \beta_{ij}\cos\Delta_{ij}\right), \\ A_{i,N+1} &= \frac{1}{2\pi}\sum_{j=1}^{N}\left(\cos\Delta_{ij}\ln D_{ij} - \beta_{ij}\sin\Delta_{ij}\right), \\ A_{N+1,j} &= \frac{1}{2\pi}\left(\beta_{1,j}\sin\Delta_{1j} + \beta_{N,j}\sin\Delta_{Nj} - \cos\Delta_{1j}\ln D_{1j} - \cos\Delta_{Nj}\ln D_{N,j}\right) \\ A_{N+1,N+1} &= \frac{1}{2\pi}\sum_{j=1}^{N}\left(\sin\Delta_{1j}\ln D_{1j} + \sin\Delta_{Nj}\ln D_{N,j} + \beta_{1j}\cos\Delta_{1j} + \beta_{Nj}\cos\Delta_{Nj}\right) \\ b_i &= V_\infty\sin\left(\theta_i-\alpha\right),\ i=1,\ldots,N, \\ b_{N+1} &= -V_\infty\cos(\theta_1-\alpha) - V_\infty\sin(\theta_N-\alpha), \end{aligned}$$

where $\Delta_{ij} = \theta_i - \theta_j$. For more details see [1, 2].

Linear system (9) provides the values of γ and q_j, using which the tangential components of velocity are computed:

$$u_{\tau i} = u_i\cos\theta_i + v_i\sin\theta_i.$$

The local pressure coefficient on the discretized profile is computed from

$$C_{p,i} = 1 - \left(\frac{u_{\tau i}}{V_\infty}\right)^2. \quad (10)$$

The hydrodynamic forces acting on the boundary element Ej are given by:

$$\begin{aligned} f_{xj} &= C_{p,j}\left(y_{j+1}-y_j\right), \\ f_{yj} &= C_{p,j}\left(x_{j+1}-x_j\right). \end{aligned} \quad (11)$$

The total force is the sum of contributions of each boundary element:

$$F_x = \sum_{j=1}^{N}f_{xj},\ F_y = \sum_{j=1}^{N}f_{yj}. \quad (12)$$

Lift coefficient is then given by:

$$C_L = -F_x\sin\alpha + F_y\cos\alpha. \quad (13)$$

Next phase after the computation of the velocity distribution in potential flow around the profile consists in the computation of boundary layer parameters divided into two sub-steps: laminar boundary layer and turbulent boundary layer [5-7]. The boundary layer starts at the stagnation point and follows the profile along the upper or lower surface in direction of trailing edge (fig. 3).

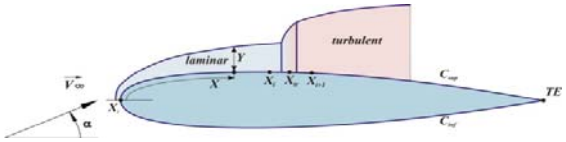

Figure 3. Transition from laminar to turbulent boundary layer.

The computation of laminar boundary layer parameters is based on the Von Karman integral-differential momentum equation:

$$\frac{d\theta}{dx}+\frac{\theta}{V}\left(2+\frac{\delta^*}{\theta}\right)\frac{dV}{dx}=\frac{1}{2}C_f, \qquad (14)$$

where V represents the velocity of the boundary layer exterior part in the considered point, δ^* is the displacement thickness, θ is the momentum thickness and C_f denotes the local friction coefficient on the profile surface. Introducing shape parameter $H=\delta^*/\theta$, allows to rewrite equation (14) as follows:

$$\frac{d\theta}{dx}+(2+H)\frac{\theta}{V}\frac{dV}{dx}=\frac{1}{2}C_f. \qquad (15)$$

Introducing the kinetic energy thickness θ^* Von Karman equation (14) leads to

$$\frac{d\theta^*}{dx}+3\frac{\theta^*}{V}\frac{dV}{dx}=2C_d, \qquad (16)$$

where C_d denotes the dissipation coefficient. Introduce in (16) the second shape parameter $H^*=\theta^*/\theta$ to get:

$$\theta\frac{dH^*}{dx}+H^*(H-1)\frac{\theta}{V}\frac{dV}{dx}=2C_d-\frac{1}{2}H^*C_f. \qquad (17)$$

In order to determine all boundary layer parameters, equations (15) and (17) are coupled with Falkner-Skan semi-empirical correlations between H^* and H, [6]:

$$H^*=\begin{cases}0.076\dfrac{(H-4)^2}{H}+1.515, & \text{if } H<4,\\ 0.04\dfrac{(H-4)^2}{H}+1.515, & \text{otherwise.}\end{cases} \qquad (18)$$

Also, let $\mathrm{Re}_\theta=\mathrm{Re}\cdot\theta\cdot V$ and assume that

$$\frac{1}{2}\mathrm{Re}_\theta C_f=F_1(H),\ 2\mathrm{Re}_\theta\frac{C_d}{H^*}=F_2(H),$$

where

$$F_1=\begin{cases}0.01977\dfrac{(H-7.4)^2}{H-1}-0.067, & \text{if } H<7.4,\\ 0.022\dfrac{(H-7.4)^2}{(H-6)^2}-0.067, & \text{otherwise,}\end{cases} \qquad (19)$$

$$F_2=\begin{cases}0.00205(4-H)^{11/2}+0.207, & \text{if } H<4,\\ \dfrac{-0.003(H-4)^2}{1+0.02(H-4)^2}+0.207, & \text{otherwise.}\end{cases} \qquad (20)$$

Multiply equation (15) by Re_θ and let $\omega=(\mathrm{Re}_\theta)^2$. Re-arrange terms to obtain:

$$\frac{1}{2}V\frac{d\omega}{dx}+(2+H)\omega\frac{dV}{dx}=F_1(H). \qquad (21)$$

Multiply equation (17) by Re_θ/H^* and re-arrange terms to get:

$$\omega V\frac{d(\ln H^*)}{dH}\frac{dH}{dx}+(1-H)\omega\frac{dV}{dx}=F_2-F_1. \qquad (22)$$

Then, equations (21) and (22) are rewritten as follows

$$\begin{aligned}&\frac{1}{2}V(x)\frac{d\omega}{dx}+(2+H)\omega A(x)=F_1(H),\\ &\omega V(x)F_3(H)\frac{dH}{dx}+(1-H)\omega A(x)=F_4(H),\end{aligned} \qquad (23)$$

where

$$A(x)=\frac{dV}{dx},$$
$$F_3(H)=\frac{d(\ln H^*)}{dH},$$
$$F_4(H)=F_2(H)-F_1(H).$$

The system of nonlinear ODE (23) coupled with initial conditions

$$\omega(0)=\frac{F_1(2.24)}{4.24A(0)},$$
$$H(0)=2.24,$$

is solved by backward Euler method, in which functions F1 and F4 are linearized in vicinity of Hj. Method is iterated till either the transition from the laminar layer to the turbulent layer is predicted or trailing edge TE is reached.

The transition from laminar to turbulent boundary layer is located by Michel criterion, [8]. Let $\mathrm{Re}_x=\mathrm{Re}Vx$ and

$$\mathrm{Re}_{\theta\max}=1.174\left(1+\frac{22.4}{\mathrm{Re}_x}\right)\mathrm{Re}_x^{0.46}. \quad (24)$$

Then, transition takes place if $\mathrm{Re}_\theta>\mathrm{Re}_{\theta\max}$ with transition point being the root of linear interpolation of $\mathrm{Re}_\theta(x)-\mathrm{Re}_{\theta\max}(x)$.

The computations of the turbulent boundary layer parameters are done by applying the Head's model based on the Von Karman integral equations for turbulent boundary layer, [6]. Let Q denote the flow volume in the boundary layer at an arbitrary point x, $\delta^*=\delta-Q/V$ be the displacement thickness and $E=d\left(V\theta H_1\right)/dx$ be the entrainment velocity. According to the Head's model the dimensionless velocity E/V depends only on H_1, that in its turn, depends only on H. Cebeci and Bradshow [6] have considered the empirical relations

$$E/V=0.0306(H_1-3)^{-0.6169}, \quad (25)$$

$$H_1=\begin{cases}0.8234(H-1.1)^{-1.287}+3.3, H\le 1.6,\\ 1.5501(H-0.6778)^{-3.064}+3.3, H>1.6\end{cases} \quad (26)$$

Last equation to determine the unknowns θ, H, H_1 and C_f is the Ludwieg-Tillman wall friction law:

$$C_f=\frac{0.246}{10^{0.678H}\,\mathrm{Re}_\theta^{0.268}}. \quad (27)$$

Combining Von Karman integral equation and relations (25)–(27) provides a system of ODE:

$$\frac{dY}{dx}=g(Y,x), \quad (28)$$

where $Y=\begin{bmatrix}\theta & H_1\end{bmatrix}^T$ and

$$g(Y,x)=\begin{bmatrix}-\frac{\theta\left(H_1+2\right)}{V}\frac{dV}{dx}+\frac{1}{2}C_f\\ -\frac{H_1}{V}\frac{dV}{dx}-\frac{H_1}{\theta}\frac{d\theta}{dx}+\frac{0.0306}{\theta\left(H_1-3\right)^{0.6169}}\end{bmatrix}.$$

The initial values are the final values supplied by the laminar boundary layer step. The numerical integration of system (28) is done by Runge-Kutta method of order 2, namely:

$$Y^*=Y_j+h_jg(Y_j,x_j),$$
$$Y_{j+1}=Y_j+h_j\left(\frac{1}{2}g(Y_j,x_j)+\frac{1}{2}g(Y^*,x_j)\right),$$

that is iterated either till the trailing edge is reached or till the separation of the turbulent layer occurs. The drag coefficient C_D is computed from Squire-Young formula [9]:

$$C_D=2\left(\theta V^\lambda|_{x_{TE},C_{upper}}+\theta V^\lambda|_{x_{TE},C_{lower}}\right), \quad (29)$$

where $\lambda=\left(H|_{x_{TE}}+5\right)/2$.

4. TORQUE AND FORCES ACTING ON THE MULTI-BLADE HYDRODYNAMIC ROTOR

Consider a rotor with diameter 4 m and 5 hydrodynamic blades with NACA 0016 symmetrical profile with chord length 0,8 m and height 1,4 m. The numerical methods, described in previous section, are used to compute the hydrodynamic coefficients $C_{L,ref}$ and $C_{D,ref}$ for the symmetrical profiles selected from the NACA library of aerodynamic profiles with a reference chord length $c_{ref}=1\,m$. The coefficients corresponding to the profile with the chord length 0,8 m are calculated from the relations:

$$C_L=1,3C_{L,ref},\ C_D=1,3C_{D,ref}.$$

The magnitude of the hydrodynamic force $\vec{F}$ acting on the blade, its tangential and normal components $F_{x'}$ and $F_{y'}$ versus the positioning angle are presented in fig. 4 (a). Fig. 4 (b) shows the torque $T_{r,i}$ developed by a single blade versus the positioning angle.

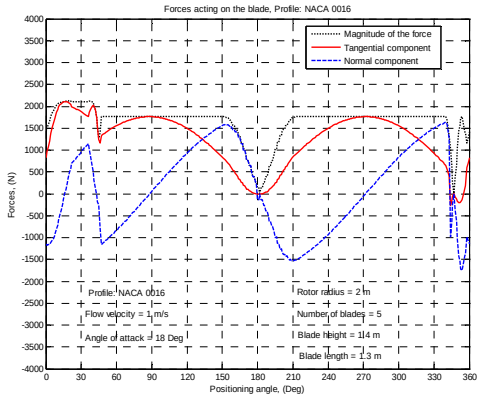

(a)

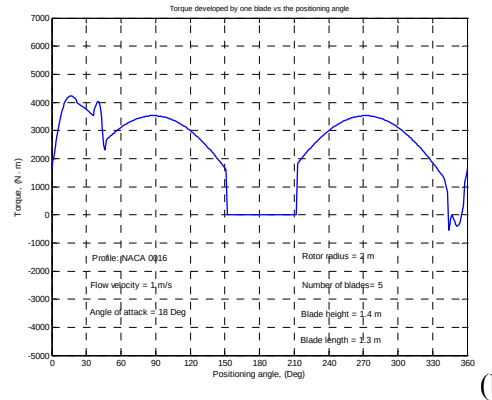

(b)

Figure 4. Hydrodynamic force components (a) and torque (b) versus the positioning angle.

Fig. 5 (a) shows the total torque at the rotor shaft $T_{r\Sigma}$ developed by all blades versus the

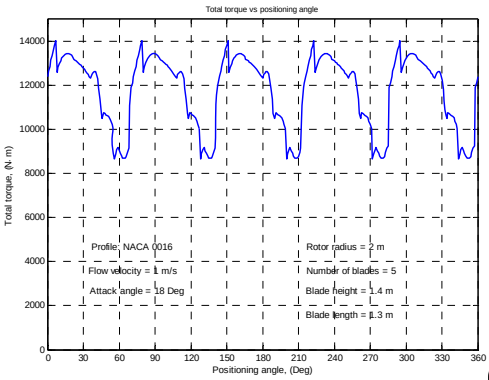

(a)

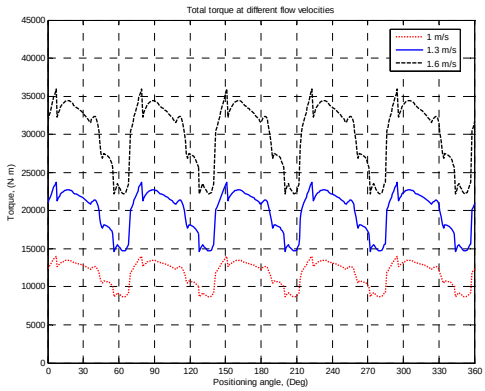

(b)

Figure 5. Total torque developed by 5 blades (a) and total torque for various flow velocities (b).

positioning angle, while Fig. 5 (b) shows the total torque $T_{r\Sigma}$ for three water flow velocities V_∞ .To determine the optimal working angle of attack it is necessary to compute the value of the torque for several values of the angle of attack: $\alpha = 15^o,\ 17^o,\ 18^o,\ 20^o,$ (fig. 6).

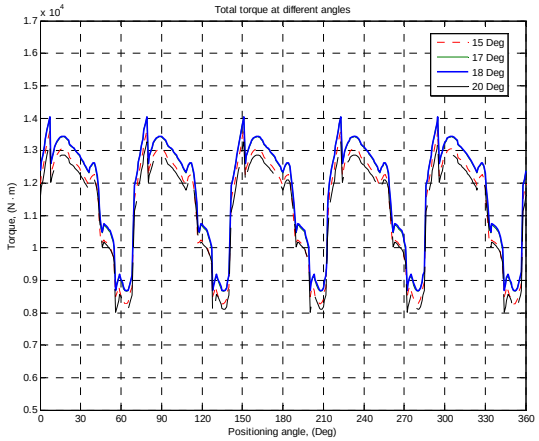

Figure 6. Torque developed by 5 blades versus the positioning angle.

5. HYDRODYNAMIC BLADE WITH SCREENS FOR DIRECTING THE FLUID FLOW IN THE BOUNDARY LAYER

Consider a laminated composite material shell composed of the following layers as shown in fig. 7: first layer bidirectional lining of type E fiberglass and polyetheric resin matrix; second layer has two sub-layers consisted of chopped fiberglass linings with an armoured polypropylene lining between them; third layer is again a chopped fiberglass lining in a polyetheric matrix; and the fourth is a gelcout covering layer.

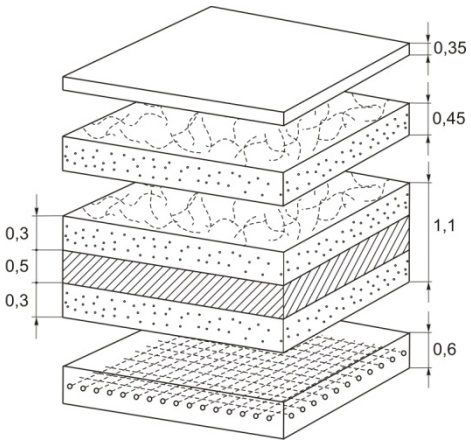

Figure 7. The structure of the composite material blade cover.

The computation of the material constants was performed using the manufacturer recommendations. The Young modulus for the

composite layer is $E = E_m V_m + E_f V_f$, where E_m and E_f are Young modulus for matrix and fiberglass, respectively, and V_m and V_f are the volume fractions of the matrix and fiberglass, [10]. Poisson coefficient is computed similarly. Thus, the following values have been obtained: Young modulus $E = 13,2GPa$ and Poisson coefficient $\nu_{12} = 0,3$.

Two FEM models have been considered: a section of the hollow blade discretized with finite elements Solsh190 and a section of the blade injected with polyurethane foam (density $0,6kg/cm^3$, $E = 0,95GPa$, $\nu = 0,24$) discretized with Solsh190 elements (lateral cover) and Solid45 elements (interior), [11, 12]. In both cases the lateral cover is made of laminated composite materials with thickness 2,6mm. The blade is subjected to hydrodynamic forces corresponding to the flow velocity of 2m/s and hydrostatic pressure. The maximum value of the forces acting on the blade is 11 kN. In the hollow hydrodynamic blade with composite material cover with thickness 2,6mm the maximal displacement is 4,3mm and the maximal stress value is approximately 38MPa. The stresses and displacement distributions are similar with those of hollow blade with aluminum cover. In fig. 8 there are presented displacements and the main stresses in the injected with polyurethane foam blade with the same thickness of lateral cover: displacements u_x (a), u_y (b) and u_z (c), and main stresses σ_1 (d), σ_2 (e) and σ_3 (f). While carrying out research on Computational Fluid Dynamics (CFD) of blade-fluid interaction it was stated the existence of fluid turbulent flow in the boundary layer, the intensity of which depends on its flow speed. To reduce the influence of this phenomenon on the conversion efficiency it is proposed to equip the blades with screens *1* for directing fluid flow in the boundary layer. Screens are spaced from one another at distance $h_b = \frac{1}{6}(V+1)$ and their peripheral profile is the equidistance with prominence

$$e = \tau_e c,$$

where c is the length of the blades chord, V is the flow velocity and parameter

$$0,02c \le \tau_e \le 0,06c .$$

Constructively the blade (fig. 9) consists of modules *2* with height h_b separated by screens *1*. Each module consists of sub-modules *3* with common composite coating. Modules *2* and

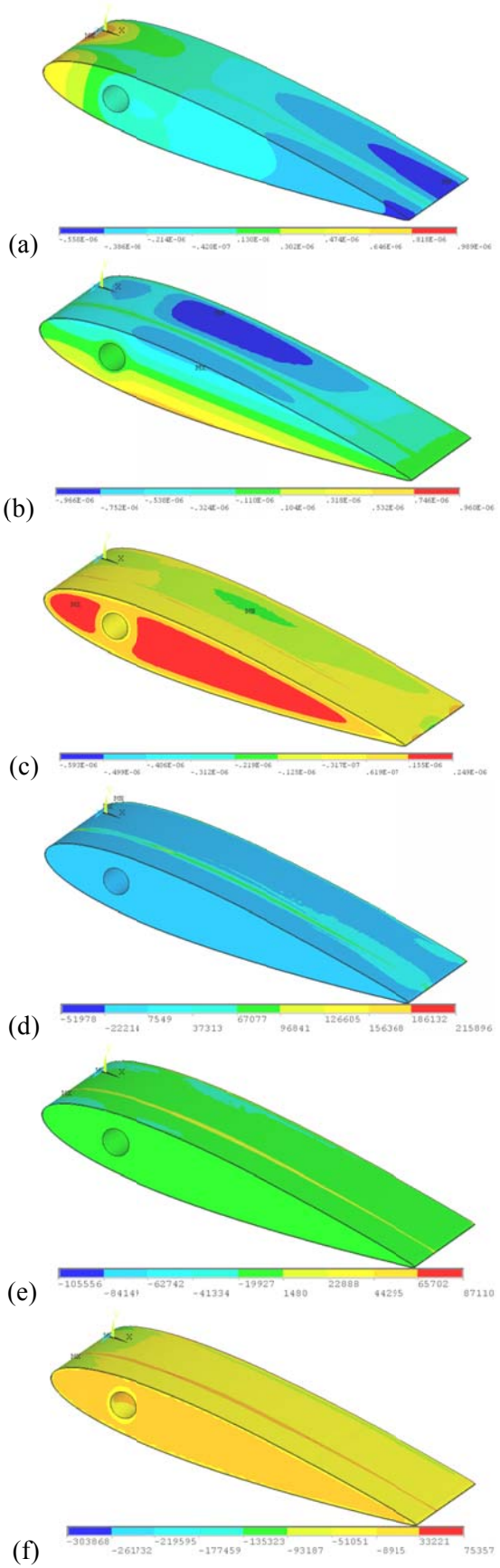

Figure 8. Displacements and main stresses in the blade injected with polyurethane foam and composite material cover with thickness 2,6 mm: u_x (a), u_y (b), u_z (c), σ_1 (d), σ_2 (e) and σ_3 (f).

screens *1* are assembled on a common shaft *4* mounted in levers *5* of rotor and fixed to rod *6*. The number of modules is determined depending on the total height *H* of the blade.

To manufacture the composite material side cover of modules *2* with hydrodynamic profile, the reversed (mirror) profile moulds (fig. 10) were executed using numerical control milling machine with 5 degree mobility. Fig. 11 shows the manufacturing of a blade (a, b) and the general view of a finished blade with modified hydrodynamic profile, manufactured on the basis of composite materials technologies.

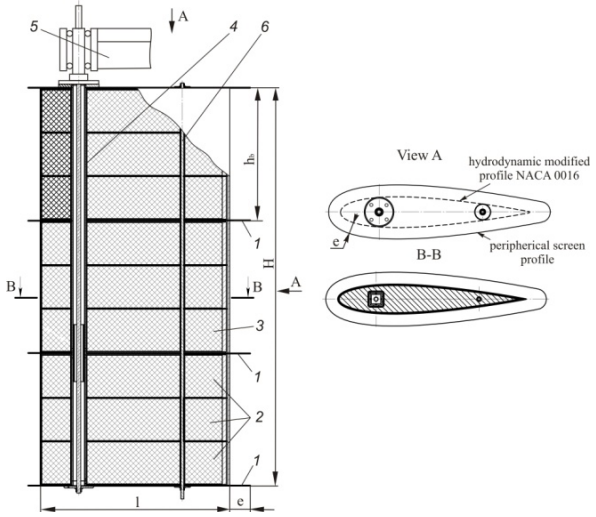

Figure 9. Blade construction.

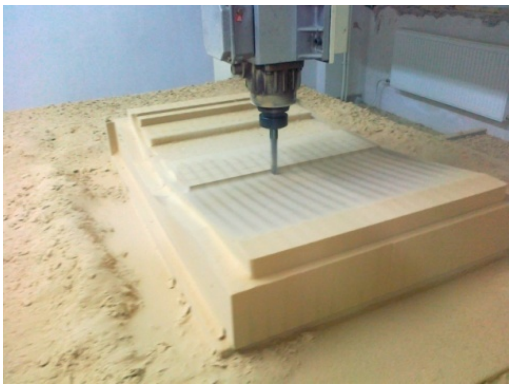

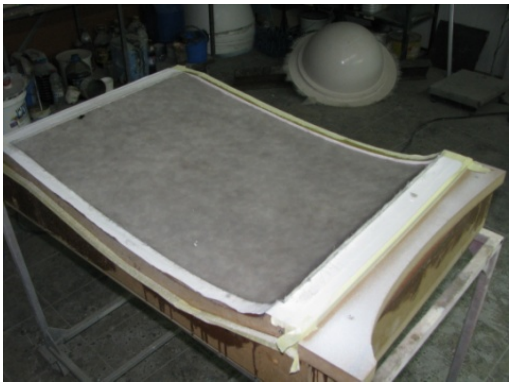

Figure 10. Manufacturing of reverse moulds.

(a)

(b)

(c)

Figure 11. Hydrodynamic blade manufacturing (a, b) and finished blade (c).

6. DIFFERENTIATED ORIENTATION MECHANISM OF BLADES

To increase energy conversion the blades *3* must be oriented towards the fluid flow direction at a variable angle of attack α, depending on the passed area (upstream, downstream and transition areas). For this purpose on the semi shaft *4* of each blade *3* (fig. 12) a rod *5* is attached placed perpendicular to the blade cord respectively and equipped with two rotating sleeves *6* located with the possibility of changing distance *l* from the blade semi shaft.

Guides *7*, *8* and *9* are mounted at rotor periphery, and rotating sleeves *6* roll in contact on their guide surface. The profile of guides and their position with respect to the location of rotor centre defines the angle of attack α and the evolution of its change for each blade during a full rotation. Thus, any blade in each point of its circular motion path is positioned at the same angle of attack α. At any point of the motion trajectory of the blades *3*, angle α can be modified depending on the flow velocity V_∞ by varying the location parameter *l* of the rotating bodies *6* to the semi shaft axes *4* of blades *3*.

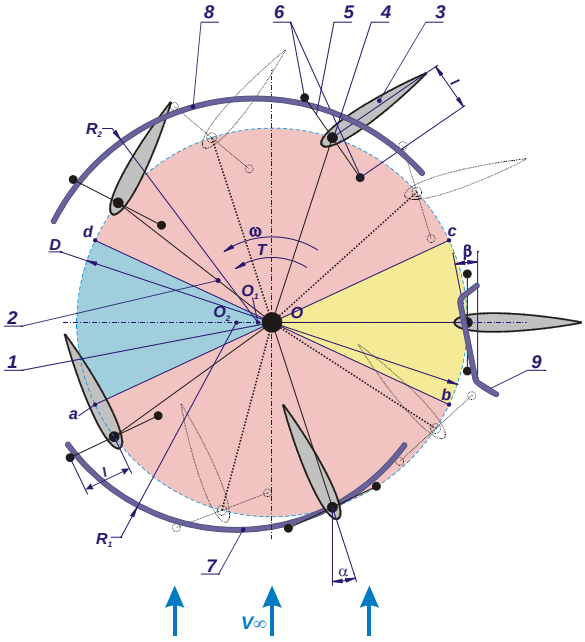

Figure 12. Differentiated orientation mechanism of blades.

Based on carried out research the optimal hydrodynamic profile and angle of attack were identified; their differentiated orientation mechanism was designed with account of requirements and constructive-kinematical solutions specified below.

Profile of guides *7*, *8* and *9* and their location shall provide individual positioning of each blade under optimal differentiated angle of attack α depending on the area of the blade-fluid interaction considering the flow rate of water flow. This condition is achieved by: location in the upstream area *Oab* of the rotor of circular guide *7* with radius R_1 and with the origin in the centre O_1 moved at distance OO_1; location in the downstream area *Ocd* of another circular guide *8* with radius R_2 and with the origin in the centre O_2 moved at distance OO_2, and in the upstream-downstream transition area by location of the rectilinear guide *9* positioned under angle β with respect to the flow direction. In this case the interaction of the rotating sleeves *6* of rods *5* with the guide profile, the blades are positioned in order to ensure that hydrodynamic forces developed by blades in all three areas *Oab*, *Ocd* and *Oda* contribute to torque development of the rotor shaft *1*, that in its turn will lead to increased energy conversion efficiency.

Also, in order to ensure the stability of blades *3* positions during their interaction with the fluid, semi shafts *4* are placed on the axis of symmetry of the hydrodynamic profile at distance $|BW|$ (fig. 13) from the blade edge determined from relation:

$$|BW| = 0,25c - k, \text{ with } \Delta \le k \le k_{\max}$$

Where c is the length of the blade chord, k is the distance ensuring condition of stability of blade positioning in fluid

$$R_k > 0, \tag{30}$$

$\Delta \in [25,40]mm$ denotes the parameter that depends of chord length c change in the interval (800–1300) mm, and k_{max} is the maximum distance determined from the condition ensuring admissible friction forces in the kinematic coupling rotating sleeve- guide.

In case of blade rotation $0 < \varphi < 2\pi$ at a variable angle of attack α, the orientation mechanism of blades should ensure stability of their positioning (fig. 13), which can be achieved if the reaction force in the kinematical coupling rotating sleeve – guide satisfies condition (30). On the other side, from the condition of minimizing unnecessary friction forces in kinematic couplings rotating sleeve – guide it follows that

$$R_{k,\max} = \tau R_k, \tag{31}$$

where $R_{k.\max}$ is the maximum reaction in the kinematic couplings rotating sleeve – guide and

parameter $\tau \in [1,2,\ 1,5]mm$. Reaction R_k in higher order kinematical coupling sleeve – guide can be expressed by relation:

$$R_k = \frac{F_L h}{l}, \tag{32}$$

where F_L is the hydrodynamic force developed at blade-fluid interaction, h is the distance between the blade semi shaft axes and the action line of the hydrodynamic force, and l denotes the distance between the blade semi shaft axes and sleeve (rotating body).

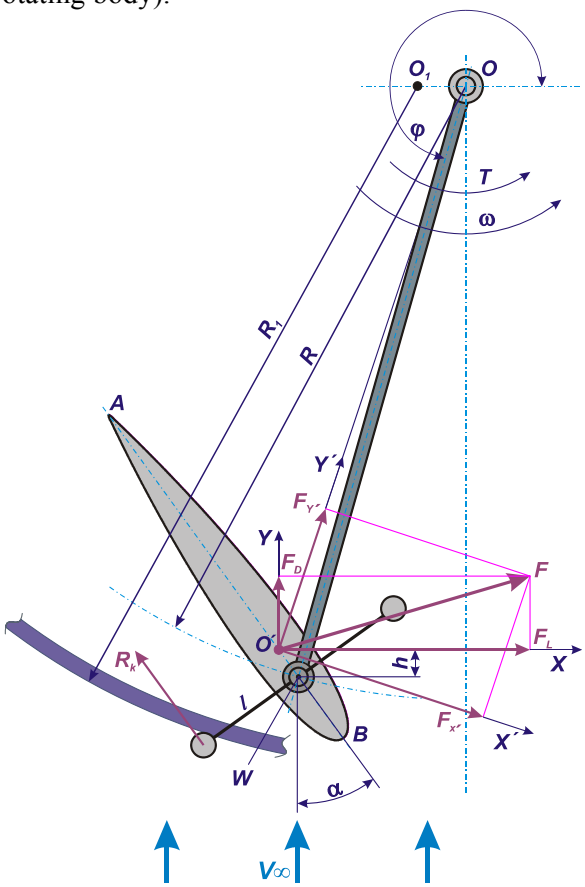

Figure 13. Stability of blade positioning in orientation mechanism.

From relation (32) results that in order to ensure the stability of blade positioning in its rotational motion in the fluid while respecting condition (30), it is necessary to identify the point W of location of blade semi shaft as well as the influence of the pitch moment, the turbulence regime, boundary layer parameters etc.

Installation of rotating bodies *6* in rods *5* with possibility of changing their distance l from the blades *3* semi shaft axis *4* ensures repositioning of blades depending on the flow rate of water flow, and thus provides conversion efficiency increase.

Profile shape of guides *7*, *8* and *9* and their location calculated with regard of rotor diameter D, and with consideration of the influence of the flow velocity of water flow on the correct positioning of blades, ensures in the result blades *3* orientation at variable angles of attack α depending on the area of blade-fluid interaction, namely:

- in upstream area *Oab*: $12^o \le \alpha \le 25^o$;
- in downstream area *Ocd*: $25^o \le \alpha \le 90^o$;
- in the upstream to downstream transition area *Obc*: $12^o \le \alpha \le 90^o$.

Differentiated positioning of the blades under variable angle of attack provides increased energy conversion by efficient exploiting of hydrodynamic forces developed by blades and reducing hydraulic resistance forces acting on the blades in their rotation around the hydraulic rotor main shaft.

7. CONCLUSIONS

The hydraulic turbine with 5 hydrodynamic profile blades assures conversion of 49.5% of the energetic potential of water stream with velocity 1.3 m/s. The optimal orientation of the blades with respect to water stream direction (enabled by differentiated orientation mechanism) assures participation of all blades (even those moving upstream) in generating the torque at the rotor shaft.

The modular blades with composite materials cover injected with polyurethane foam and resistance structure with 4 transversal screens assure minimal local deformations and prevents an early boundary layer separation that will not influence significantly the water flow and efficiency of energy conversion. Experimental testing of the micro hydropower station MHCF D4x1,5E in real field conditions confirmed that the hydropower station with hydrodynamic 5−blade rotor assures the conversion of the energy at the rotor shaft to the generator clams with efficiency of 77.5%.

Bibliography

1. Bostan V. *Computational Analysis of Hydrodynamic Effects in Hydraulic Flow Turbines (Part 1), Annals of University of Craiova, Electrical Engineering series, No.35, 2011, pp.83-92.*

2. Bostan I., Gheorghe A., Dulgheru V., Sobor I., Bostan V., Sochirean A. *Resilent Energy Systems. Renewables: Wind, Solar, Hydro, Topics in Safety, Risk, Reliability and Quality, Vol. 19, Springer, 2012.*

3. Moran J. *An Introduction to Theoretical and Computational Aerodynamics, John Wiley and sons, 1984.*
4. Katz J., Plotkin A. *Low Speed Aerodynamics, From Wing Theory to Panel Methods, Mac-Graw Hill, 1991.*
5. Batcelor G.K. *An Introduction to Fluid Dynamics, Cambridge University Press, 1970.*
6. Cebeci T., Bradshaw P*. Momentum Transfer in Boundary layers, Hemisphere Publishing Corportation, 1977.*
7. Reynolds W.C., Cebeci T. *Calculation of Turbulent Flows, Topics in Applied Physics Series, Springer-Verlag, Vol.12, 1978.*
8. Michel R. *Etude de la Transition sur les Profiles d'Ales, Onera Report, 1/1578A, 1951.*
9. Squire H.B., Young A.D. *The Calculation of the Profile Drag of Aerofoils, R.&M.1838, ARC Technical Report , London, 1938.*
10. Jones R. M. *Mechanics of Composite Materials, 2nd Edition, Taylor & Francis, 1999.*
11. *ANSYS 10.0, User's Guide.*
12. *ANSYS 10.0, Advanced Analysis Techniques Guide.*

Recommended for publication> 21.02.2013.